

FLUID STRUCTURE INTERACTION IN FULLY COLLAPSIBLE TUBES

Maršík F.* ,Štembera V., Chlup H., Hemza J.

*Author for correspondence

Institute of Thermomechanics Czech Academy of Sciences,

Dolejšková 5,

182 00 Prague 8,

Czech Republic,

E-mail: marsik@it.cas.cz

ABSTRACT

The main goal of the developed theory is to formulate the biomechanical conditions (geometrical dimensions, viscoelastic properties of veins and blood fluid flow conditions) at which an unstable behavior or even the vein collapse can occur. The above problems are numerically modeled by the finite element method. The weak formulation of the tube deformation is based on the virtual work principle. The mixed formulation of the finite element method with the separately interpolated pressure is used for the structure. The strong coupling of both structure and fluid solvers allow us to simulate self-induced large deflection oscillations of the tube.

Provided that the Neo-Hook's material model was applied the analytical formula for the collapse conditions was found. It was proved that for the brain vein contraction about 5%, the vein collapse can occur even under normal physiological condition – the angiosynizesis.

The fluid structure interaction is studied experimentally on the special experimental line. The fluid structure phenomenon is investigated both for the continuous and pulsating flow and it is evaluated by a non-invasive optical. The method is based on optical measurements of radial displacement of the pulsating tube wall.

The simultaneous clinics observation (histological findings), in vitro experiments and numerical modeling gives sufficient data to predict biomechanical conditions of the angiosynizesis.

INTRODUCTION

In human biomechanics are the structure changes of blood vessels important in many physiological situations; e.g., pressure pulse propagation in arteries, collapse of highly elastic bridging brain veins, vein walls oscillations during pulsating flow, etc. [1]. Fluid structure phenomenon is highly dependent on the material properties of veins and blood and moreover on the velocity field structure before and behind the deformed cross-section. The accurate and well-formulated fluid-structure problem is up to now mainly elaborated for the steady state

flow, for pressure pulse propagation and aneurysma growth [2, 6]. The description of such phenomenon like Korotkoff sounds (the sounds heard during measurement of blood pressure) is very difficult and it needs to include the response of relevant part of the all cardiovascular system. The lumped 1D simulations give some chance too [5]. The adequate explanation is not entirely done up to now. The main reason of this study is to find some relation between *the onset of the self-induced oscillations and the blood flow conditions together with the material properties* of the veins. Such phenomena like pulse propagation, self-induced oscillations and collapse are clinically well indicated.

In general, two approaches for FSI (Fluid Structure Interaction) are applied – the monolithic and the partitioned approach. In the monolithic approach both sets of equations, describing the fluid and the structure, are solved together as a single system of equations. The formulation is often based on the weak solution of the balance laws in the ALE (Arbitrary Lagrangian Eulerian) formulation [6]. The corresponding nonlinear system of algebraic equations is solved e.g., by Newton's method. In some numerical realizations the GMRES (General Minimal Residual Method) is applied, to provide good precondition for the solution of the corresponding linear systems. However, to save the numerical stability some additional tricks are needed. For example, the block-triangular approximations of the Jacobian matrix, obtained by neglecting selected fluid–structure interaction blocks were used in [3]. The monolithic approach is more straightforward from the mathematical point of view; nevertheless, it can bring problems in practice. One is due to the attempt to capture within one discretization procedure the completely different spatial and temporal characteristics of the flow and the structure, which can lead to an ill-conditioned system of equations. Another problem is that sometimes it is difficult to test the solvers separately (flow through rigid tube test, etc.). Nevertheless, the monolithic approach is intensively studied and some

satisfactory results of numerical simulation should be reached [2, 6].

The partitioned approach, which uses two separate solvers for fluid and structure, contrary to the monolithic approach, has to transfer the values between both solvers on each time level.

Two ways are possible – the so-called strong coupling strategy, where the balance of momentum is reached on each time level using sub iterations, and the weak coupling strategy, sometimes also referred to as the loose coupling strategy, where both solvers are run only once in each time step and no balance of forces is guaranteed. The latter approach is suitable only in cases where the momentum transferred between both solvers is small, for example for the pressure pulse propagation, aneurysm growth or in aeroelasticity problems. This paper is concentrated to the strong coupling strategy to find the onset of self-induced oscillation (generated by a positive feedback). The flow is for simplicity supposed as 1D and the vein is taken as a 3D structure under finite deformations [8].

The analytical, more qualitative analysis elucidates the simple relation between elastic modulus of vein and the blood flow rate. Both numerical simulation and analytical conclusions are compared with experiments [7].

NOMENCLATURE

$\mathbf{a}_0, \mathbf{g}_0$	[1]	unit vectors describing fiber directions
a_k, b_k	[1]	shape functions
A, A_0	[m ²]	actual, initial cross-sectional area of the tube, resp.
c	[m s ⁻¹]	speed of disturbance, sound speed
\mathbf{c}^{-1}	[1]	Finger deformation tensor
$\mathbf{C} = \mathbf{F}^T \mathbf{F}$	[1]	Green deformation tensor
$\mathbb{C}, \bar{\mathbb{C}}$	[J m ⁻³]	elasticity tensors,
dV	[m ³]	volume element
D, D_0	[m]	actual, initial tube diameter, resp.
\mathbb{D}	[J m ⁻³]	auxiliary tensor
f	[s ⁻¹]	frequency
\mathbf{f}	[N m ⁻²]	external surface force
$\mathbf{F} = \partial \mathbf{x} / \partial \mathbf{X}$	[1]	the deformation gradient
\mathbf{G}	[1]	Lagrange deformation tensor
h	[m]	distance between two neighboring nodes
h_0	[m]	thickness of the tube wall
I_1, I_2, I_3	[1]	invariants of tensor \mathbf{C}
$j = \det \mathbf{F} $	[1]	determinant of the \mathbf{F}
J_4	[1]	anisotropy pseudo-invariant (Gent model)
J_m	[1]	fiber extensibility parameter (Gent model)
k	[m ⁻¹]	wave number
\mathbf{K}		stiffness matrix
K_p	[Pa]	tube stiffness coefficient
l, l_0	[m]	actual, initial length of flexible tube, resp.
m	[kg]	mass
\mathbf{M}	[kg]	mass matrix
n_{LS}	[1]	number of load steps
N_e, N	[1]	number of elements, number of element nodes
\mathcal{N}	[1]	node index set
N_p, N_q	[1]	number of pressure or displacement unknowns

p	[Pa]	static pressure in fluid
\bar{p}	[Pa]	pressure computed from displacement
\mathbf{q}	[m]	discretized displacement vector
Q	[m ³ s ⁻¹]	flow rate
\mathbf{r}	[N]	vector of external forces
r, ϑ, z		cylindrical coordinates
R, R_0	[m]	actual, initial radius of the tube, resp.
Re, Re_{crit}	[1]	actual, critical Reynolds number, resp.
s	[J kg ⁻¹ K ⁻¹]	entropy
S	[Js]	action
\mathbf{S}, \mathbf{S}_0	[1]	second Piola-Kirchhoff stress, prestress tensor, resp.
\mathbf{t}, \mathbf{t}_0	[Pa]	Cauchy stress, prestress tensor, resp.
T	[K], [s]	temperature, time period
T_z	[N]	tube tension
\mathbf{u}	[m]	displacement vector
\mathbf{v}	[m s ⁻¹]	fluid velocity
V, V_0	[m ³]	actual, initial volume, resp.
u	[J kg ⁻¹]	internal energy
\mathbf{x}, \mathbf{X}	[m]	actual, initial position, resp.
α	[1]	material exponent
γ	[rad m ⁻¹]	relative distortion
δ_{ij}	[1]	Kronecker's delta symbol
ε	[1]	element index set
ε_R	[1]	fluid-structure relaxation parameter
κ	[Pa]	compressibility modulus
λ, λ_f	[1]	relative extension, frictional coefficient
μ	[Pa]	shear modulus
μ_d	[Pa s]	dynamic viscosity
μ^{aniso}, J_m^{aniso}	[Pa], [1]	Gent anisotropic material parameters
$\nu = \mu_d / \rho$	[m ² s ⁻¹]	kinematic viscosity
ρ, ρ_0	[kg m ⁻³]	actual, initial density, resp.
τ, τ_{fluid}	[s]	FSI time step, time step for fluid solver
$\theta_1, \phi_1, \theta_2, \phi_2, \beta$	[rad]	fiber orientation angles
Ψ	[J m ⁻³]	strain energy function (isochoric + volumetric parts)
$\Psi_{iso}, \Psi_{vol}, \Psi_{totc}$	[J m ⁻³]	strain energy function (isochoric, volumetric, total)
ω	[s ⁻¹]	angular velocity

HAMILTONIAN AND VARIATIONAL PRINCIPLES-BALANCE LAWS

The deformation of a solid elastic body can be formulated on the base of the Hamiltonian principle

$$S = \int_{t_0}^t \int_{V_0} \rho_0 \left[\frac{1}{2} \left(\frac{\partial \mathbf{u}_I(\mathbf{X}, t)}{\partial t} \right)^2 - u(s(\mathbf{X}, t), \mathbf{G}(\mathbf{X}, t)) - \phi(\mathbf{X}) \right] dV dt \quad (1)$$

where $\mathbf{u}(\mathbf{X}, t) = \mathbf{x}(\mathbf{X}, t) - \mathbf{X}$ is displacement of material point \mathbf{X} into position $\mathbf{x}(\mathbf{X}, t)$, dV is a volume element Figure 1. The measure of the deformation in material description is Lagrange deformation tensor \mathbf{G} , or

$$G_{ij}(\mathbf{X}, t) = \frac{1}{2} \left(\frac{\partial u_i}{\partial X_j} + \frac{\partial u_j}{\partial X_i} + \frac{\partial u_i}{\partial X_i} \frac{\partial u_j}{\partial X_j} \right), \quad \text{for } i, j = 1, 2, 3 \quad (2)$$

(Einstein summation rule is applied.) Internal energy of material point is $u(s(\mathbf{X}, t), \mathbf{G}(\mathbf{X}, t))$ and depends on the entropy $s(\mathbf{X}, t)$ and on the deformation. $\phi(\mathbf{X})$ is the density of the potential energy. The entropy is not well measurable quantity, but can be used as a measure of the process irreversibility.

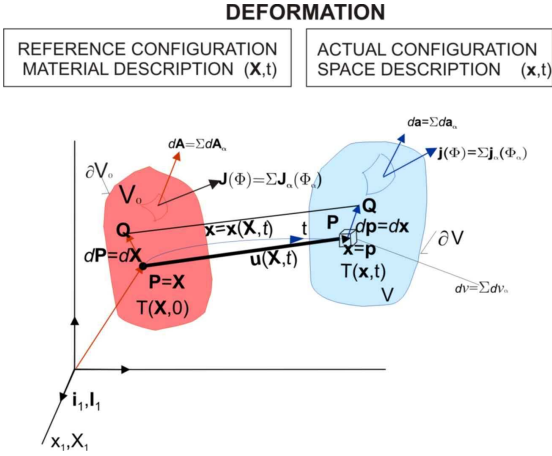


Figure 1 Deformation of a continuum body with initial volume V_0 into actual volume V .

The first variation of this functional with respect to the material point trajectory $\mathbf{x}(\mathbf{X}, t)$ is

$$\delta S = \int_{t_0}^t \int_{V_0} \rho_0 \delta l(\mathbf{u}(\mathbf{X}, t), \mathbf{X}) dv dt, \text{ for } \delta \mathbf{x}(\mathbf{X}, t) = \delta \mathbf{u}(\mathbf{X}, t) \quad (3)$$

$$\delta l(\mathbf{X}, t) = \frac{\partial u_i}{\partial t} \frac{\partial \delta u_i}{\partial t} - \left[\left(\frac{\partial u}{\partial \mathbf{G}} \right)_s \frac{\partial \mathbf{G}}{\partial u_i} + \left(\frac{\partial u}{\partial s} \right)_G \frac{\partial s}{\partial u_i} + \frac{\partial \phi}{\partial u_i} \right] \delta u_i$$

The body density $\rho_0(\mathbf{X})$ in the reference configuration does not depend on the deformation. The volume forces are expressed by the gradient $-\partial \phi / \partial u_i$, where vector $\mathbf{u} = (u_1, u_2, u_3)$ is the displacement. Due to the definition of internal energy the variation of it is equal

$$\delta u = \left(\frac{\partial u}{\partial s} \right)_G \delta s + \left(\frac{\partial u}{\partial \mathbf{G}} \right)_s \delta \mathbf{G} = T \delta s + \frac{\mathbf{S}}{\rho_0} \delta \mathbf{G} \quad (4)$$

where \mathbf{S} is the second Piola-Kirchhoff stress tensor. The entropy can be split into reversible (i.e., equilibrium) and irreversible (i.e., non-equilibrium) parts

$$T \delta s = T \delta s_{eq} + T \delta s_{ir} \quad (5)$$

We omit the irreversible part of the entropy for our purpose; it results in the neglecting of such irreversible processes, like viscoelasticity, thermal conductivity and chemical reactions. Including definitions (4) and integrating per partes the variation of (3) can be written in the form

$$\delta S = \int_{V_0} \rho_0 \frac{\partial u_i}{\partial t} \delta u_i dv \Big|_{t_0}^t - \int_{t_0}^t \int_{V_0} \left[\rho_0 \frac{\partial^2 u_i}{\partial t^2} + \mathbf{S} \frac{\partial \mathbf{G}}{\partial u_i} + \rho_0 T \frac{\partial s_{eq}}{\partial u_i} + \rho_0 \frac{\partial \phi}{\partial u_i} \right] \delta u_i dv dt = 0 \quad (6)$$

The displacement variation $\delta \mathbf{u}(\mathbf{X}, t) = \delta \mathbf{x}(\mathbf{X}, t)$, which is equivalent to the material point trajectory variation, see Figure 1, is at the beginning and at the end of deformation equal zero, i.e., the first integral in the variation (6) is zero. When the

necessary condition of extreme (6) is valid for each time $t \in (t_0, t)$ we obtain the extended virtual work principle

$$\int_{V_0} \left[\rho_0 \frac{\partial^2 u_i}{\partial t^2} + \mathbf{S} \frac{\partial \mathbf{G}}{\partial u_i} + \rho_0 T \frac{\partial s_{eq}}{\partial u_i} + \rho_0 \frac{\partial \phi}{\partial u_i} \right] \delta u_i dv = \int_{V_0} \rho_0 \left(\frac{\partial^2 u_i}{\partial t^2} + \frac{\partial \phi}{\partial u_i} \right) \delta u_i dv + \int_{V_0} \delta \psi(T, \mathbf{G}) dv = 0 \quad (7)$$

Applying this virtual work principle, the arbitrary virtual displacements $\delta \mathbf{u}$ are assumed. When they are in directions of the displacement of material point \mathbf{X} the **balance of momentum** is satisfied and when they are orthogonal to the constraint forces (which is not usually this case, so this derivation works only for special cases), the constraint forces do no work.

The function variation

$$\delta \psi(s, \mathbf{G}) = \left[\left(\mathbf{S} \frac{\partial \mathbf{G}}{\partial u_i} \right)_s + \rho_0 T \left(\frac{\partial s_{eq}}{\partial u_i} \right)_G \right] \delta u_i \quad (8)$$

is the strain energy density change induced by the external surface forces and by the internal processes. This strain energy density is composed from the pure elastic energy (isentropic processes only) and thermal energy generated by thermoelasticity.

The total external surface force $\mathbf{f} = (f_1, f_2, f_3)$ effecting on the actual surface ∂V in the actual configuration is

$$\int_{\partial V} f_i(\mathbf{x}, t) da = \int_{\partial V} t_{ji}(\mathbf{x}, t) da_i = \int_{V_0} j t_{ji}(\mathbf{x}, t) \frac{\partial X_k}{\partial x_i} dA_k = \int_{V_0} \frac{\partial}{\partial X_k} T_{ki}(\mathbf{X}, \mathbf{x}, t) dv, \text{ for } T_{ki}(\mathbf{X}, \mathbf{x}, t) = j \frac{\partial X_k}{\partial x_i} t_{ji}(\mathbf{x}, t), \quad (9)$$

$$\text{or } S_{ij}(\mathbf{X}, t) = j \frac{\partial X_i}{\partial x_k} \frac{\partial X_j}{\partial x_l} t_{kl}(\mathbf{x}, t),$$

$$\text{where } j = \det \left| \frac{\partial x_k}{\partial X_l} \right| = \det |\mathbf{F}|, \quad \mathbf{F} = \frac{\partial \mathbf{x}}{\partial \mathbf{X}}, \quad \mathbf{F}^{-1} = \frac{\partial \mathbf{X}}{\partial \mathbf{x}}$$

Here $t_{ji}(\mathbf{x}, t)$ is the Cauchy stress tensor and $T_{ki}(\mathbf{X}, \mathbf{x}, t)$ is the first Piola-Kirchhoff stress and $S_{ij}(\mathbf{X}, t)$ is the second Piola-Kirchhoff stress tensor. The corresponding external mechanical energy loaded on the body is

$$\left(\frac{\partial}{\partial X_k} S_{ik}(\mathbf{X}, t) + \rho_0 \frac{\partial \phi}{\partial u_i} \right) \delta u_i = 0 \quad (10)$$

The first term is the influence of the surface force and the second term is generated by the external potential energy (e.g., gravitational, centrifugal etc.) The condition is applicable for a static analysis only.

The formula (9) is applied for the formulation of the external boundary conditions as well. In our case of the flexible tube the most important external force is the static pressure $p(\mathbf{x}, t)$, i.e., $t_{ij} = p \delta_{ij}$. The condition of the virtual work (7) has to be completed by the external mechanical energy

$$\int_{\partial V_0} j t_{ii}(\mathbf{x}, t) \frac{\partial X_k}{\partial x_i} \delta u_i dA_k = \int_{\partial V_0} j p \delta_{ij} \frac{\partial X_k}{\partial x_i} \delta u_j dA_k \quad (11)$$

which is included as the boundary conditions on the surface ∂V_0 . The balance of the mass is not included up to now. In this integral formulation it is necessary to add mass balance as the additional constraint to the virtual principle (7). The initial density $\rho_0(\mathbf{X})$ changes during deformation to the actual density $\rho(\mathbf{x}, t)$ by the formula

$$\rho_0 = j\rho, \text{ or } \frac{\rho - \rho_0}{\rho_0} = \frac{1-j}{j} \quad (12)$$

The equation (12) is the formulation of *the balance of mass*, where $j = \det(\mathbf{F}) = \rho_0 / \rho$. The change of density is completely determined by the deformation gradient \mathbf{F} or alternatively by the Lagrange deformation tensor (2). Finally, to the strain energy density has to be added the mechanical energy containing the term $(1-j)\delta p$, where p is static pressure (its physical meaning is the density of mechanical energy and serves here like Lagrange multiplier). The pressure p is included like another new variable included in the strain energy function. As it is commonly used, the strain energy Ψ is divided in the three parts

$$\Psi_{\text{total}}(T, \mathbf{G}) = \Psi_{\text{iso}}(T, \mathbf{G}) + \Psi_{\text{vol}}(T, \mathbf{G}) - \frac{(\bar{p}-p)^2}{2\kappa}, \quad (13)$$

for $\bar{p} = -\frac{d\Psi_{\text{vol}}}{dj}$, $j = \det(\mathbf{F})$, $2\mathbf{G} = \mathbf{F}^T \mathbf{F} - \mathbf{I}$

the isochoric part Ψ_{iso} and the volumetric part Ψ_{vol} , and an additional term, which relates to the pressure p and to the pressure \bar{p} computed from displacements. The parameter κ serves as a penalty parameter and is usually equal to the compressibility modulus. The final form of the virtual work principle (7) is

$$\int_{V_0} \left[\left(\rho_0 \frac{\partial^2 \mathbf{u}_j}{\partial t^2} \delta_{jk} + r_k \right) + \left(\frac{\partial \Psi}{\partial G_{ij}} - \frac{\bar{p}-p}{\kappa} \frac{\partial \bar{p}}{\partial G_{ij}} \right) \frac{\partial G_{ij}}{\partial \mathbf{u}_k} \right] \delta \mathbf{u}_k dV = 0, \quad (14)$$

$$\text{where } r_k(\mathbf{u}) = -\rho_0 \frac{\partial \phi}{\partial \mathbf{u}_k} \quad \text{for } j=1,2,3$$

$$\int_{V_0} \frac{\bar{p}-p}{\kappa} \delta p dV = 0 \quad (15)$$

Temperature T is taken as a constant.

MODEL FORMULATION

The fluid-structure interaction problem is not possible to solve analytically in general. Due to its complexity we have to apply some numerical method. Usually, the combination of the finite difference method (used for time dependence) and the finite element method (for space dependence) is exploited. This approach is widely studied for its advantages to include the materials that are slightly or entirely incompressible and anisotropic. Materials are considered hyperelastic, slightly

compressible and are described by the strain energy function Ψ .

A two-field approximation is used, the problem unknowns being displacement \mathbf{u} and the separately interpolated pressure p .

In this paper we use three materials – the Neo-Hookean, the isotropic Gent and the anisotropic Gent material. We note that the strain energy function of all materials in this paper is independent of invariant I_2 (the second invariant of the right Cauchy-Green strain tensor \mathbf{C}). Firstly, we have to derive expressions for the strain-energy function Ψ of these materials, the corresponding hydrostatic pressure \bar{p} with its derivatives, the second Piola-Kirchhoff stress tensor \mathbf{S} and the elasticity tensor \mathbb{C} .

Neo-Hookean Model

It is the simplest hyperelastic model described by one parameter (isochoric part) and the simplest material model belonging to the Mooney-Rivlin material family. The parameter μ has a straightforward physical meaning; it is equal to the material shear modulus, which can be proven by the small strain limit. The model is defined by the strain energy function

$$\Psi_{\text{iso}} = \frac{\mu}{2} \ln \left(j^{-\frac{2}{3}} I_1 - 3 \right), \quad \Psi_{\text{vol}} = \frac{\kappa}{2} (j-1)^2 \quad (16)$$

Isotropic Gent Model

The model is based on the assumption of limiting fiber extensibility, which holds for some organic materials, such as tissues. The fibers are stretched up to some length, where their stiffness starts to grow by several orders of magnitude. This behavior is simply modeled by the logarithmic function. The Gent model is often used for its simplicity – only two material parameters with a straightforward physical meaning are needed. The model is described by the strain energy function

$$\Psi_{\text{iso}} = -\frac{\mu J_m}{2} \ln \left(1 - \frac{j^{-\frac{2}{3}} I_1 - 3}{J_m} \right), \quad \Psi_{\text{vol}} = \frac{\kappa}{2} \left(\frac{j^2 - 1}{2} - \ln j \right) \quad (17)$$

Anisotropic Gent Model

We introduce an anisotropic Gent model that is often used for simulating real artery walls. The model is based on the assumption of limiting fiber extensibility. The function describing anisotropy is deduced directly from the isotropic Gent model. A material is modeled as a composite reinforced with two families of helical fibers, whose directions are defined by two unit vectors \mathbf{a}_0 and \mathbf{g}_0 . The model consists of the isotropic Neo-Hookean model with an additional term describing anisotropy, denoted by $\Psi_{\text{iso}}^{\text{aniso}}$

$$\Psi_{\text{iso}} = \frac{\mu}{2} \ln \left(j^{-\frac{2}{3}} I_1 - 3 \right) + \Psi_{\text{iso}}^{\text{aniso}}, \quad \Psi_{\text{vol}} = \frac{\kappa}{2} (j-1)^2 \quad (18)$$

Let us focus only on this term

$$\Psi_{\text{iso}}^{\text{aniso}} = -\mu^{\text{aniso}} J_m^{\text{aniso}} \ln \left[1 - \left(\frac{J_4 - 1}{J_m^{\text{aniso}}} \right)^2 \right], \quad J_4 = \frac{I_4 + I_6}{2} \quad (19)$$

where

$$\begin{aligned} I_4 &= \mathbf{a}_0 \cdot \mathbf{C} \mathbf{a}_0 = (\mathbf{a}_0 \otimes \mathbf{a}_0) : \mathbf{C}, \\ I_6 &= \mathbf{g}_0 \cdot \mathbf{C} \mathbf{g}_0 = (\mathbf{g}_0 \otimes \mathbf{g}_0) : \mathbf{C} \end{aligned} \quad (20)$$

FINITE ELEMENT FORMULATION

We shall find the solution of the fluid-structure interaction as the extreme conditions (14) and (15) by the finite element method. The problem is to calculate a new unknown configuration, induced by a different load vector (11) i.e., by the external surface force generated by the fluid flow or by the volume force \mathbf{r} . The set of the linear algebraic equations can be created either for a steady-state problem or for one time-step of a time-dependent problem. The variation of the total strain energy (14) with respect to the displacement \mathbf{u} , and a variation of the total strain energy with respect to the pressure p (15) have to be zero. The whole initial body volume V_0 will be divided into N_e finite elements, which have N global element nodes. The global number of the nodes of the pressure approximation is N_p .

Let us come from the continuous variables \mathbf{u}, p to their discrete counterparts $q_1, q_2, \dots, q_{N_q}, p_1, p_2, \dots, p_{N_p}$ defined by the approximations

$$\mathbf{u}_1 \approx \sum_{k=1}^{N_q} a_k(x, y, z) q_k, \quad \mathbf{u}_2 \approx \sum_{k=1}^{N_q} a_{k+N}(x, y, z) q_{k+N}, \quad (21)$$

$$\begin{aligned} \mathbf{u}_3 &\approx \sum_{k=1}^{N_q} a_{k+2N}(x, y, z) q_{k+2N}, \\ p &\approx \sum_{k=1}^{N_p} b_k(x, y, z) p_k \end{aligned} \quad (22)$$

The fluid-structure interaction is dynamic process and the coefficients $q_1, q_2, \dots, q_{N_q}, p_1, p_2, \dots, p_{N_p}$ depend on the time.

Steady State Solution

To show the coupling between displacement \mathbf{u} and pressure p we start with the steady problem, which is defined by

$$\int_{V_0} \left[\left(\frac{\partial \Psi}{\partial G_{ij}} \frac{\bar{p}-p}{\kappa} \frac{\partial \bar{p}}{\partial G_{ij}} \right) \frac{\partial G_{ij}}{\partial u_k} - r_k \delta u_k \right] dV = 0, \quad j = 1, 2, 3 \quad (23)$$

$$\int_{V_0} \frac{\bar{p}-p}{\kappa} \delta p dV = 0 \quad (24)$$

Approximation (21) and (22) in equations, (14) and (15) gets

$$\int_{V_0} \left(\frac{\partial \Psi}{\partial G_{ij}} \frac{\bar{p}-p}{\kappa} \frac{\partial \bar{p}}{\partial G_{ij}} \right) \frac{\partial G_{ij}}{\partial q_k} \delta q_k dV - r_k \delta q_k = 0, \quad j = 1, 2, 3 \quad (25)$$

$$\int_{V_0} \frac{\bar{p}-p}{\kappa} b_k \delta p_k dV = 0 \quad (26)$$

Let us now consider that equations (25) and (26) are defined in the new unknown configuration (which we now denote by the superscript $n+1$). Let us approximate all variables in these equations by values from the old configuration (denoted by no superscript) using the Taylor theorem

$$\bar{p}^{n+1} = \bar{p} + \frac{\partial \bar{p}}{\partial G_{ij}} \frac{\partial G_{ij}}{\partial q_r} \Delta q_r, \quad p^{n+1} = p + \Delta p,$$

$$\left(\frac{\partial \Psi}{\partial G_{ij}} \right)^{n+1} = \frac{\partial \Psi}{\partial G_{ij}} + \frac{\partial^2 \Psi}{\partial G_{ij} \partial G_{rs}} \frac{\partial G_{rs}}{\partial q_n} \Delta q_n,$$

$$\left(\frac{\partial G_{ij}}{\partial q_k} \right)^{n+1} = \frac{\partial G_{ij}}{\partial q_k} + \frac{\partial^2 G_{ij}}{\partial q_k \partial q_r} \Delta q_r,$$

$$\left(\frac{\partial \bar{p}}{\partial G_{ij}} \right)^{n+1} = \frac{\partial \bar{p}}{\partial G_{ij}} + \frac{\partial^2 \bar{p}}{\partial G_{ij} \partial G_{rs}} \frac{\partial G_{rs}}{\partial q_r} \Delta q_r.$$

Let us denote

$$S_{ij} := \frac{\partial \Psi}{\partial G_{ij}}, \quad \mathbb{C}_{ijkl} := \frac{\partial^2 \Psi}{\partial G_{ij} \partial G_{kl}} \quad (27)$$

where \mathbf{S} is the second Piola-Kirchhoff stress tensor and \mathbb{C} is the elasticity fourth-order tensor.

If we neglect all second order terms and omit $\delta q_k, \delta p_k$, we get the set of linear algebraic equations which bring into effect the extreme conditions (23)

$$\begin{aligned} &\left\{ \int_{V_{0e}} \left[\frac{\partial G_{ij}}{\partial q_k} \mathbb{D}_{ijmn} \frac{\partial G_{mn}}{\partial q_r} + S_{ij}^{pg} \frac{\partial^2 G_{ij}}{\partial q_k \partial q_r} \right] dV \right\} \Delta q_r + \\ &+ \left\{ \int_{V_{0e}} \frac{1}{\kappa} \frac{\partial \bar{p}}{\partial G_{ij}} \frac{\partial G_{ij}}{\partial q_k} b_d dV \right\} \Delta p_d = \\ &= r_k - \int_{V_{0e}} S_{ij}^{pg} \frac{\partial G_{ij}}{\partial q_k} dV, \quad k = 1, \dots, N_q \end{aligned} \quad (28)$$

where b_d are the by coefficients for the pressure interpolation, for $d = 1, 2, \dots, N_p$ and $r = 1, 2, \dots, N_q$, see equations (21), (22).

Moreover from the condition (24) we have

$$\begin{aligned} &\left\{ \int_{V_{0e}} \frac{1}{\kappa} \frac{\partial \bar{p}}{\partial G_{ij}} \frac{\partial G_{ij}}{\partial q_r} b_k dV \right\} \Delta q_r - \left\{ \int_{V_{0e}} \frac{b_k b_d}{\kappa} dV \right\} \Delta p_d = \\ &- \int_{V_{0e}} \frac{\bar{p}-p}{\kappa} b_k dV, \quad k = 1, \dots, N_p \end{aligned} \quad (29)$$

where we have defined the following two tensors

$$\mathbb{D}_{ijmn} = \mathbb{C}_{ijmn} - \frac{1}{\kappa} \frac{\partial \bar{p}}{\partial G_{ij}} \frac{\partial \bar{p}}{\partial G_{mn}} - \frac{\bar{p}-p}{\kappa} \frac{\partial^2 \bar{p}}{\partial G_{ij} \partial G_{mn}}, \quad (30)$$

$$i, j, m, n = 1, 2, 3, \quad S_{ij}^{pg} = S_{ij} - \frac{\bar{p}-p}{\kappa} \frac{\partial \bar{p}}{\partial G_{ij}}, \quad i, j = 1, 2, 3$$

Values of N and N_p are given according to the number of the finite elements and the order of displacement approximation and according to the corresponding pressure approximation.

Denoting the matrix coefficients by \mathbf{K} and external forces by \mathbf{f} , the equations (28) and (29) written for the whole volume $V_0 = \sum_c V_{0c}$ can be written in the form:

$$\begin{aligned} \mathbf{K}_{uu}(\mathbf{q})\Delta\mathbf{q} + \mathbf{K}_{up}(\mathbf{q})\Delta\mathbf{p} &= \mathbf{f}_u, \\ \mathbf{K}_{up}^T(\mathbf{q})\Delta\mathbf{q} + \mathbf{K}_{pp}(\mathbf{q})\Delta\mathbf{p} &= \mathbf{f}_p \end{aligned} \quad (31)$$

We have obtained the set of linear algebraic equations for the deformation and pressure increments $\Delta\mathbf{q}$, $\Delta\mathbf{p}$, respectively. The elimination of the pressure increments gets the global system of equations for the static deformation.

Static Condensation of Pressure

Due to the fact that the separately interpolated pressure is not forced to be continuous between elements, it can be condensed out on the element level. Then the global vector of unknowns contains only displacements, as it is the case in the displacement based method. A pressure value can be reconstructed from displacements whenever needed. The local system of equations (28), (29), constructed on each element, can be written in the form

$$\begin{aligned} \mathbf{K}_{uu}\Delta\mathbf{q} + \mathbf{K}_{up}\Delta\mathbf{p} &= \mathbf{f}_u, \\ \mathbf{K}_{up}^T\Delta\mathbf{q} + \mathbf{K}_{pp}\Delta\mathbf{p} &= \mathbf{f}_p \end{aligned} \quad (32)$$

from which we obtain

$$\Delta\mathbf{p} = \mathbf{K}_{pp}^{-1}(\mathbf{f}_p - \mathbf{K}_{up}^T\Delta\mathbf{q}) \quad (33)$$

and finally

$$(\mathbf{K}_{uu} - \mathbf{K}_{up}\mathbf{K}_{pp}^{-1}\mathbf{K}_{up}^T)\Delta\mathbf{q} = \mathbf{f}_u - \mathbf{K}_{up}\mathbf{K}_{pp}^{-1}\mathbf{f}_p \quad (34)$$

From the local system of equations (34), given for each element, the global system of equations is built:

$$\mathbf{K}(\mathbf{q})\Delta\mathbf{q} = \mathbf{f}(\mathbf{q}) \quad (35)$$

3.3. FLUID FLOW INTERACTION- DYNAMIC CASE

The coefficients \mathbf{q} in the displacement approximation (21) depend on the time. The inertial effects are included in the extended virtual work principle (14) and (15). The inertia term has in this approximation form

$$\delta\mathbf{u}^T \int \rho_0 \ddot{\mathbf{u}} dv = \delta\mathbf{q}^T \left\{ \int \rho_0 \mathbf{N}^T \mathbf{N} dv \right\} \ddot{\mathbf{q}} = \delta\mathbf{q}^T \mathbf{M}_V \ddot{\mathbf{q}}, \quad (36)$$

$$\text{for } \mathbf{M}_V = \int_{V_{0e}} \rho_0 \mathbf{N}^T \mathbf{N} dv$$

where matrix \mathbf{M}_V is usually called the consistent mass matrix.

Its actual form depends on the matrix \mathbf{N} , which is defined by the order of an approximation of a solution on the used finite element. Adding the inertia term (36) to the global system (35) we obtain, the system of ordinary differential equations of the second order

$$\mathbf{M}\ddot{\mathbf{q}} + \mathbf{K}(\mathbf{q}) = \mathbf{f}, \quad \dot{\mathbf{q}}(0) = \dot{\mathbf{q}}_1, \quad \mathbf{q}(0) = \mathbf{q}_0 \quad (37)$$

which, we solve by the widely used Hilber-Hughes-Taylor method. This method offers second order accuracy in time and absolute stability.

Prestressing

The material can be prestressed in the reference (initial) configuration by the Cauchy stress tensor \mathbf{t}_0 , or equivalently by the second Piola-Kirchhoff stress tensor (9), i.e.,

$$\begin{aligned} \mathbf{S}_0 &= j\mathbf{F}^{-1} \begin{pmatrix} t_{0_{11}} & 0 & 0 \\ 0 & 0 & 0 \\ 0 & 0 & 0 \end{pmatrix} \mathbf{F}^{-T} = \\ &= jt_{0_{11}} \begin{pmatrix} F_{11}^{-1}F_{11}^{-1} & F_{11}^{-1}F_{21}^{-1} & F_{11}^{-1}F_{31}^{-1} \\ & F_{21}^{-1}F_{21}^{-1} & F_{21}^{-1}F_{31}^{-1} \\ \text{sym.} & & F_{31}^{-1}F_{31}^{-1} \end{pmatrix} \end{aligned} \quad (38)$$

If, on the other hand, the prestraining of the material is given, then the value of the corresponding prestress has to be found. This value can be found for example by a numerical experiment. Then we use again formula (38).

FLUID FLOW MODEL

We introduce a mathematical model describing the fluid flow. The fluid is solved by a separate solver, which is designed to cooperate with the structural solver describing the fluid boundary. The solver is able to cooperate both with the structural solver as well as with the rigid boundary condition. This allows us to test the fluid solver separately. The model is based on the following assumptions:

- The fluid flow is one-dimensional (in space) and isothermal.
- The fluid is considered as Newtonian.
- The artificial compressibility method is used.
- The fluid flows through a tube system depicted in Figure 2.

The two rigid channels terminate the flexible part [4]. The flexible part has length l , the left rigid part and the right rigid part have equal length l_0 . The cross-sectional area of the tube is denoted by $A(x,t)$, the cross-sectional area of the rigid parts is denoted by A_0 . The fluid flows from the reservoir with

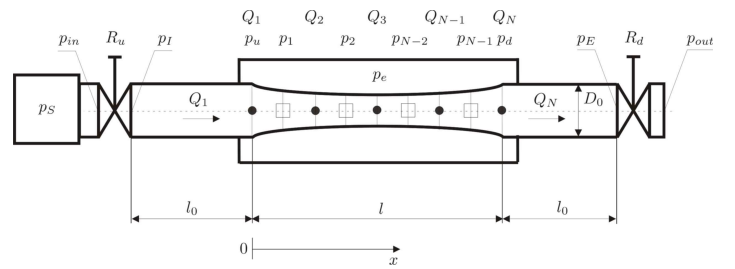


Figure 2 Schematic diagram of the modeled tube system – (• - flow rate discretization points, □ - pressure discretization points)

constant pressure p_s . The pressures at the beginning and at the end of the left rigid part are denoted by p_l and p_u , respectively, and analogously the pressure at the beginning and

at the end of the right rigid tube is denoted by p_d and p_E , respectively. There are two non-reflecting elements (restrictors) in the system, one at the beginning of the left rigid part and the second one at the end of the right rigid part.

The flexible part of the tube is located within a box with constant pressure p_e . The pressure at the input to the left restrictor is denoted by p_{in} and the pressure at the output from the right restrictor is denoted by p_{out} . **The tube deformation (flexible part) is modeled by a full three-dimensional approach, in contrary to the one-dimensional approach used in the presented fluid model.**

FLOW TROUGH FLEXIBLE TUBE

The model is one-dimensional in space, i.e. all quantities depend on time t and the space variable x , the values of which are supposed to be constant across the cross-section. The standard balance laws have the following form:

$$\frac{\partial A}{\partial t} + \frac{\partial(Av)}{\partial x} = 0, \quad (39)$$

$$\frac{\partial v}{\partial t} + v \frac{\partial v}{\partial x} + \frac{1}{\rho} \frac{\partial p}{\partial x} = \underbrace{-\frac{\lambda_f S}{8 A}}_f v|v| \quad (40)$$

where $p = p(x,t)$ is the fluid pressure, $v = v(x,t)$ is the fluid velocity, $A = A(x,t)$ is the tube cross-section, $S(x) = \pi D(x)$ is the circumference of the tube and f [N/kg] is the volume force representing viscous losses in the tube.

At the end of tube, the flow through the rigid tube (i.e., $A(x,t) = A_0 = const$) is solved, see Figure 2. From the equation (39) follows, that the velocity in the tube is constant along the tube. From the equation (40) we obtain only the dependence of the flow rate $Q(t) = A_0 v(t)$ on the time. The corresponding ordinary differential equation for the rigid part has to be solved together with the equations for the middle flexible tube.

The frictional coefficient $\lambda_f = \frac{64}{Re}$ if $Re \leq Re_{krit}$ and

$\lambda_f = 1.02(\log Re)^{-2.5}$ if $Re > Re_{krit}$, where Re_{krit} is the critical

Reynolds number, for which the laminar flow becomes turbulent. The Reynolds number Re is defined as

$Re(x) = \frac{|v(x)|D_0}{\nu} = \frac{|\varrho(x)|D_0}{A(x)\nu}$, where ν [m²s⁻¹] is the kinematic

viscosity of the fluid. Our goal is to solve the equations (39) and (40) with respect to velocity v and pressure p , where cross-section A is supposed to be known. **The structure solver in each time step determines its values.** To be able to solve the system with respect to variables p and v as a system of ODEs, we use the artificial compressibility method. The balance of mass is

$$\frac{\partial A_0}{\rho c^2} \frac{\partial p}{\partial t} + \frac{\partial A}{\partial t} + \frac{\partial(Av)}{\partial x} = 0 \quad (41)$$

where c is the sound velocity in a fluid and it is taken like the parameter representing the artificial compressibility. The speed of sound $c = \sqrt{(\partial p / \partial \rho)_s}$ in the water is 1494 m/s at 25° C.

The solution of the equations (41) and (40) will be done in the variables Q, p , where $Q = Av$ is the flow rate. We introduce the non-dimensional quantity $\hat{Q} = Q / Q_0$, $\hat{p} = p / p_0$, which we for simplicity denote again as Q, p . The final form of equations is

$$\begin{aligned} \frac{\partial p}{\partial t} &= -\frac{\rho c^2}{A_0 p_0} \left(\frac{\partial A}{\partial t} + Q_0 \frac{\partial Q}{\partial x} \right), \\ \frac{\partial Q}{\partial t} &= \frac{Q}{A} \left(\frac{\partial A}{\partial t} - Q_0 \frac{\partial Q}{\partial x} \right) + Q_0 \left(\frac{Q}{A} \right)^2 \frac{\partial A}{\partial x} - \frac{A}{\rho} \frac{p_0}{Q_0} \frac{\partial p}{\partial x} \\ &\quad - Q_0 \frac{\lambda_f S}{8 A^2} Q|Q| \end{aligned} \quad (42)$$

Let us discretize the system of equations in space using a staggered grid, depicted in Figure 2, with a grid step $h = l / (N - 1)$. Discretization points for the pressure p are set between the discretization points for the flow rate Q . The continuity equation is discretized in p points, whereas the balance of momentum is discretized in Q points. Moreover, we use the approximation $S \approx S_0$. We finally get

$$\begin{aligned} \dot{p}_i &= -\frac{\rho c^2}{A_0 p_0} \left(\frac{\partial A}{\partial t} \Big|_i + Q_0 \frac{Q_{i+1} - Q_i}{h} \right), \quad i = 1, \dots, N - 1 \text{ (} p \text{ points)} \\ \dot{Q}_i &= -\frac{Q}{A_i} \left(\frac{\partial A}{\partial t} \Big|_i - Q_0 \frac{Q_{i+1} - Q_{i-1}}{2h} \right) + Q_0 \left(\frac{Q_i}{A_i} \right)^2 \frac{\partial A}{\partial x} \Big|_i - \end{aligned} \quad (43)$$

$$\frac{A_i p_0}{\rho Q_0} \frac{p_i - p_{i-1}}{h} - Q_0 \frac{\lambda_f S_0}{8 A_i^2} Q_i |Q_i|, \quad i = 2, \dots, N - 1 \text{ (} Q \text{ points)}$$

FLUID-STRUCTURE COUPLING--STRUCTURE MESH AND BOUNDARY CONDITIONS

We used a structured mesh consisting of brick elements, see Figure 3. The elements are indexed by triples $(i, j, k) \in \varepsilon$, where index set ε is defined by

$$\varepsilon = \{(i, j, k); i=1, \dots, n_i, j=1, \dots, n_j, k=1, \dots, n_k\}$$

The nodes are indexed by triples $(i, j, k) \in \mathcal{N}$, where index set \mathcal{N} is defined as follows

$$\mathcal{N} = \{(i, j, k); i=0, \dots, 2n_i, j=0, \dots, 2n_j, k=0, \dots, 2n_k\}$$

which contains all vertex, mid-side, mid-face and mid-element nodes, used by quadratic element BRICK81, BRICK24 and BRICK60 skipping some of the indices; BRICK24 uses only vertex nodes and BRICK60 uses vertex and mid-side nodes only. The number behind BRICK means the number of the unknown values. The structure mesh is always set so that index i parameterizes elements in the axial direction. In case of tube geometry, index j is used in the azimuthal direction and index k in the radial direction.

Let us present two wall shapes – the block shape and the tube shape (see Figure 3). For all shapes, the following conditions are used

$$\left. \begin{aligned} \mathbf{q}(0,j,k) &= (0,0,0) \\ \mathbf{q}(2n_i,j,k) &= (q_0,0,0) \end{aligned} \right\} \forall (i,j,k) \in \mathcal{N} \quad (44)$$

where $\mathbf{q}(0,j,k)$ is the displacement vector at grid point (i,j,k) . Moreover, for the case of the quarter tube the following symmetry conditions are used:

$$q_3(i,0,k) = q_2(i,2n_j,k) = 0 \forall (i,j,k) \in \mathcal{N} \quad (45)$$

In case of the half tube we use

$$q_3(i,0,k) = q_3(i,2n_j,k) = 0 \forall (i,j,k) \in \mathcal{N} \quad (46)$$

Tube imperfections and contact algorithm

Up to now the tube cross-section was ideally circular. However, this configuration does not offer a non-symmetric solution in case of (symmetric) pressure loading, as it observed in reality. In FELIB, second and third imperfection mode can be initiated by the small parameter $\varepsilon = \pm(1 - R/R_0)$, (see Figure 3).

The possibility of wall contact is implemented only in the second collapse mode. In this case, we apriori know that the tube comes always into contact in plane $z = 0$ and that contact forces have nonzero components only in z -direction. The contact forces are searched iteratively.

FLUID-STRUCTURE INTERACTION ALGORITHM

The fluid uses a staggered grid, the advantage of which is that the fluid pressure values $p_i, i=1, \dots, N-1$ are always located in the middle of the element. Let us describe the coupling algorithm. The fluid solver needs information about the cross-sectional area of the deformed tube and its spatial and time derivatives from the structure solver at every time instant. Evaluation of the cross-section $A(x,t)$ and its derivatives has the following steps:

1. In order to get values of the cross-section and its spatial derivative in p points with high precision, the cubic natural spline is constructed from the cross-sections obtained in previous iteration.
2. The derivative of the cross-section in time is computed from cross-sections obtained at three consequent time points, using the Taylor formula. In particular, value $\frac{\partial A}{\partial t}(x_i, t_n)$ at time $t = t_n$ in point $x = x_i$ is given by
$$\frac{\partial A}{\partial t}(x_i, t_n) = \frac{3A(x_i, t_n) - 4A(x_i, t_{n-1}) + A(x_i, t_{n-2})}{2\tau} + O(\tau^3),$$
 $i = 0, \dots, 2n_i$

which guarantees second order accuracy in time.

Moreover, we define

$$A(x_i, t_{-2}) = A(x_i, t_{-1}) = A(x_i, t_0), \quad i = 0, \dots, 2n_i$$

The structure solver needs to calculate the influence of the fluid on the elastic tube, we need the fluid pressure, which is calculated from the fluid solver. Then using the structure solver (37) the iteration process of the algorithm on each time level can start. This fluid structure interaction (FSI) algorithm is written as

$$\begin{aligned} \mathbf{A}(x) &= \Phi_{\text{structure}}(\mathbf{p}(x)), \\ \mathbf{p}(x) &= \Phi_{\text{fluid}}(\mathbf{A}(x)) \end{aligned} \quad (47)$$

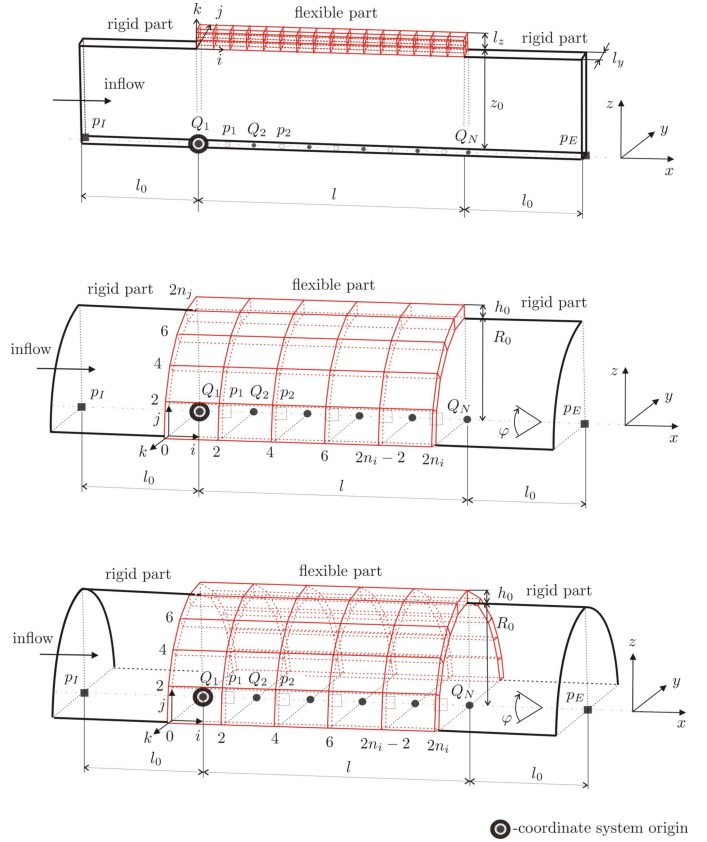


Figure 3 Connection of the fluid and structure grids created by the BRICK elements. The figure contains a nodal numbering. (above: collapsible channel, middle; quarter tube, below: half tube). Note that $2n_i = N - 1$. The imperfection is introduced by the small deformation of the initial tube radius, i.e., $(1 \pm \varepsilon)R_0$.

where $\Phi_{\text{structure}}, \Phi_{\text{fluid}}$ are the discretized structure and fluid-solver operators, respectively. We get the implicit equation

$$\mathbf{p}(x) = \Phi_{\text{fluid}}[\Phi_{\text{structure}}(\mathbf{p}(x))] \quad (48)$$

which can be solved by means of the fixed-point iterations. However, the fixed-point iterations converge slowly, therefore different modifications of this method are used in practice. We use Steffensen's method, whose algorithm is written as

$\mathbf{p}_0(x)$ is given,

$$\mathbf{p}_k(x) = \begin{cases} \mathbf{p}_{k-1}(x) \frac{(\mathbf{p}_{k-1}(x) - \mathbf{p}_{k-2}(x))^2}{(\mathbf{p}_{k-1}(x) - \mathbf{p}_{k-2}(x)) - (\mathbf{p}_{k-2}(x) - \mathbf{p}_{k-3}(x))} & \text{if } k=3,6,9,\dots \\ \Phi_{\text{fluid}}[\Phi_{\text{structure}}(\mathbf{p}_{k-1}(x))] & \text{otherwise} \end{cases} \quad k = 1, 2, \dots$$

It can be proven, that this method converges faster than fixed-point iterations, in case that the fixed-point iterations are

convergent. Let us denote the difference between the current interface pressure $\mathbf{p}(x)$ and this proposed pressure $\mathbf{p}_{\text{prop}}(x)$ as the pressure increase in the fluid $\Delta\mathbf{p}_f(x_i)$:

$$\Delta\mathbf{p}_f(x) = \mathbf{p}_{\text{prop}}(x) - \mathbf{p}(x) \quad (49)$$

Within one iteration step, the pressure is transferred from the fluid to the structure boundary only to a certain level defined by the parameter dp_{MAX} and the fluid-structure relaxation

$$\text{parameter } \varepsilon_R : \Delta\mathbf{p}(x) = \varepsilon_R \times \text{sgn}(\Delta\mathbf{p}_f(x)) \min(|\Delta\mathbf{p}_f(x)|, dp_{MAX})$$

where, for the values $\varepsilon_R = 0.5$ and $dp_{MAX} = 1000 \text{ Pa}$ $\Delta\mathbf{p}_f(x)$ is the pressure increase in the fluid from the last time step and $\Delta\mathbf{p}(x)$ is the corrected pressure increase transferred to the structure.

The numerical procedure starts with a fluid flow simulation, in which the tube is kept motionless (fixed). The fluid-structure interaction algorithm starts, when the fluid has recovered the stable Poisseuille flow, only. After that, the flexible tube is released and iterations start. In practice, the rigid tube situation is typically simulated beforehand and the final pressure and flow distributions are stored as the initial conditions.

RESULTS OF NUMERICAL SIMULATION

The actual application of the formulated FSI algorithm is shown as for the static tube collapse as for the dynamic fluid-structure interaction. To show the ability of this method, the convergence of the strong coupling iterations is demonstrated.

Let us determine the dependence of the relative tube cross-section A/A_0 on the transmural pressure $p - p_e$ in the tube

middle $\left(x = \frac{l}{2}\right)$. Both the second and the third collapse mode are simulated; the tube imperfection is set to 4% ($\varepsilon = 0.04$).

The relation between transmural pressure, which is often used in one-dimensional models and in experiments, is

$$p - p_e = K_p \left(1 - \left(\frac{A}{A_0}\right)^{-\alpha}\right) \Rightarrow \frac{A}{A_0} = \left[1 - \frac{p - p_e}{K_p}\right]^{-\frac{1}{\alpha}} \quad (50)$$

The function (50) was used for example by Hayashi [4] and with different coefficient α is used further for stability analysis.

The dependency of the form of the tube collapse on the transmural pressure for $\alpha = 3/2$ is shown in Figure 4. The lost of the structure stability (changes in the shape) has the following evolution:

- The first interesting point, marked by a triangle (Δ), is when the tube losses its structural stability and on the cross-section inflexion points appear. The cross section ratio significantly falls.
- The second interesting point is when the tube wall starts to be in contact, this point is denoted by a square (\square). From this point the cross section ratio decreases slowly.

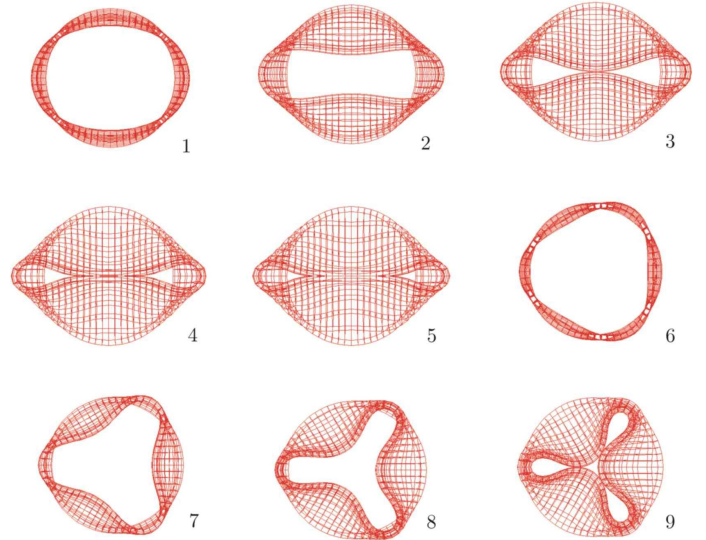
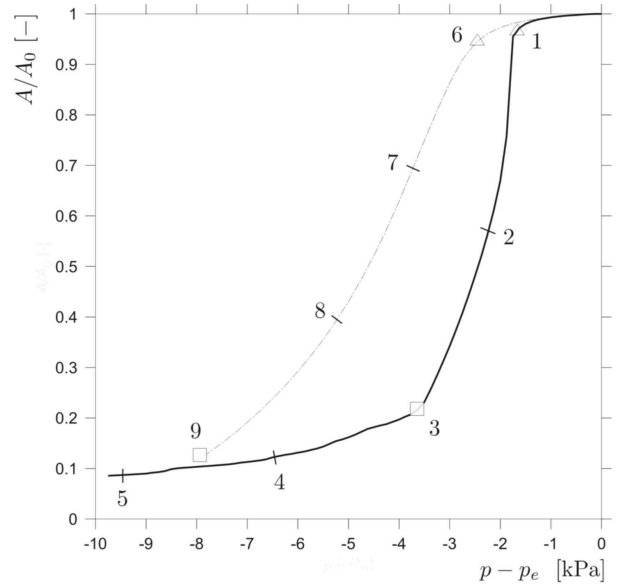


Figure 4 Static collapse of an elastic tube in the second mode (denoted by solid line, 1; $p_e = -1.75 \text{ kPa}$, 2; $p_e = -2.25 \text{ kPa}$, 3; $p_e = -3.5 \text{ kPa}$, 4; $p_e = -6.5 \text{ kPa}$, 5; $p_e = -9.5 \text{ kPa}$), and in the third mode (denoted by dot-and-dash line, 6; $p_e = -2.5 \text{ kPa}$, 7; $p_e = -3.75 \text{ kPa}$, 8; $p_e = -5.25 \text{ kPa}$, 9; $p_e = -8 \text{ kPa}$). Triangles (Δ) denote points where linear stability is lost, squares (\square) denote points of first contact between tube walls.

Flow Through Flexible Tube – Self-Excited Oscillations

The numerical simulation of FSI was provided for the anisotropic Gent material (model of arteries). The reason was to show the possible differences with respect to the isotropic material. As an interesting result was the stable self-excited low-frequency oscillations, see Figure 5. Such oscillations were only observed at the physical experiments up to now. Moreover, the numerical simulation revealed high frequency

disturbances, induced probably by the pressure waves traveling in the fluid between the ends of the tube. These disturbances cause sign changes of the flow rate and the pressure. Using an absolute value of the flow rate, the filtered quantities are obtained. The pressure and the flow rate distributions reveal self-excited oscillations with a main frequency of 23 Hz, which is a plausibly realistic estimate of the frequency obtained from experiments if we take into account that the elasticity parameter $\mu = 10$ MPa is by one order higher than the one for real latex tube used in experiment and moreover and from the distribution of Reynolds number we can see that the simulation runs in the turbulent mode. At this point, let us mention that setting the numerical solver appropriately is very important. Many simulations we tried yielded irregular oscillations without any main frequency. A sufficiently fine discretization is also important – on coarse meshes the same type of simulation was not achieved. (The simulation was run using Intel 2 GHz T7250 processor and needed more than three days to converge.)

STABILITY ANALYSIS OF THE THIN-WALLED ARTERIES AND VEINS

The numerical simulation of the flexible tube collapse is not, up to now, suitable to find the relevant quantities, which this instability causes. The analytical, even qualitative analysis is more suitable for this purpose. To find the condition of the structural instability we start with the formulation of the thin tube deformation under transmural pressure $p - p_e$ (the difference in pressure between two sides of a wall), see Figure 6. The tension T_z in the longitudinal direction induces in general, the elongation $\lambda = \frac{\partial z}{\partial Z}$ and the torsion γ , which is defined as a relative distortion $\gamma = \frac{\partial \vartheta}{\partial Z} \left[\frac{\text{rad}}{\text{m}} \right]$. For convenience the torsion angle $\tau = \gamma R$ [rad] is applied (i.e., $\text{arctg } \tau = \gamma R z / z = \gamma R$).

Under these assumptions the tube deformation is

$$r = r(R), \vartheta = \theta + \gamma Z, z = \lambda Z \quad (51)$$

and the corresponding deformation gradient has form We will suppose that the material of the blood vessel is incompressible, i.e. $j = \det \mathbf{F} = 1$, subsequently the following relation between deformation is valid

$$\frac{\partial r}{\partial R} \cdot \frac{\lambda r}{R} = 1, \text{ i.e. } \frac{\partial r}{\partial R} = \frac{R}{\lambda r} \quad (52)$$

Material Model of Veins

We apply the Neo-Hook material

$$t^{ij} = \mu \left(c^{-1ij} - \frac{C_{(1)}}{3} \delta^{ij} \right) \quad (53)$$

which is often used for description of well-flexible materials (rubber, vulcanised rubber, biological tissue). μ is shear modulus and c^{-1ij} is the Finger's strain tensor

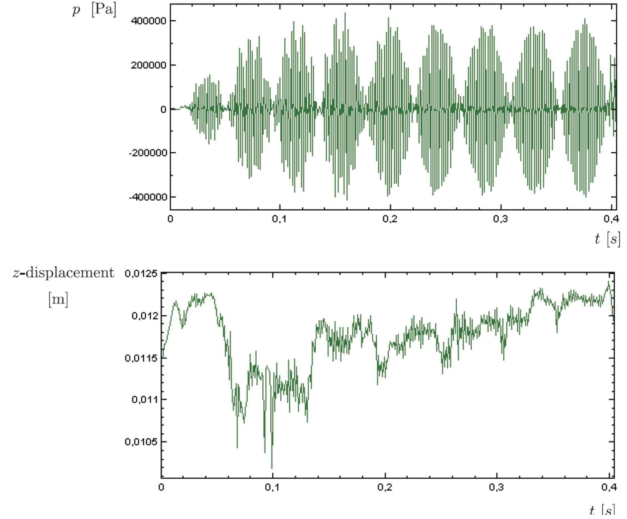


Figure 5. The self-induced oscillations of the pressure at $x = (3/4)l$ and of the z - displacement at $i = (3/2)n_i$, $x = (3/4)l, j = n_j, k = 0$, see Figure 3.

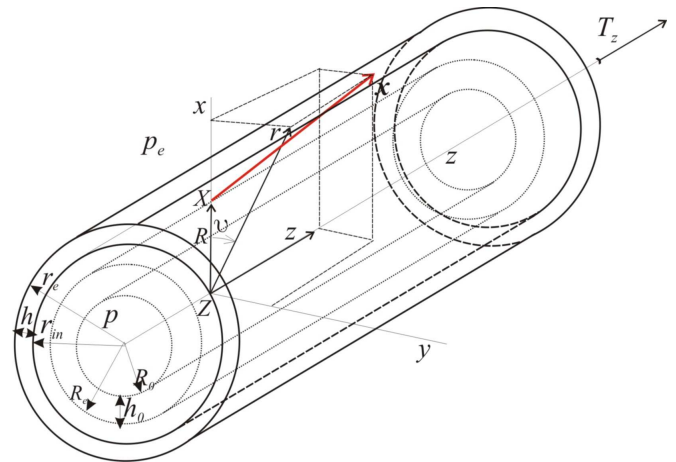


Figure 6 The inflation, torsion and the blood vessel extension. The material point shifts from the position $X = (R, \theta, Z)$ due to the deformation to the position $x = (r, \vartheta, z)$.

$$c_{ij}^{-1} = \frac{\partial x^i}{\partial X^i} \frac{\partial x^j}{\partial X^j} = \begin{pmatrix} \left(\frac{R}{\lambda r} \right)^2 & 0 & 0 \\ 0 & (\gamma R)^2 + \left(\frac{r}{R} \right)^2 & \gamma \lambda r \\ 0 & \gamma \lambda r & \lambda^2 \end{pmatrix} \quad (54)$$

The I. invariant $C_{(1)}$ of the Green's strain tensor

$$C_{ij} = \frac{\partial x^i}{\partial X^i} \frac{\partial x^j}{\partial X^j}, \text{ (or } \mathbf{C} = \mathbf{F}^T \mathbf{F} \text{) is}$$

$$C_{(1)} = C_{11} + C_{22} + C_{33} = \lambda^2 + (\gamma r)^2 + \left(\frac{R}{\lambda r}\right)^2 + \left(\frac{r}{R}\right)^2 \quad (55)$$

Finally, the Cauchy stress tensor for the Neo-Hook model (53) is

$$t_{rr} = \mu \left[\frac{2}{3} \left(\frac{R}{\lambda r}\right)^2 - \frac{r^2 + R^2(\lambda^2 + \gamma^2 r^2)}{3R^2} \right], \quad t_{r\vartheta} = t_{rz} = 0$$

$$t_{\vartheta\vartheta} = \frac{2}{3} \mu \left(\gamma^2 r^2 + \frac{r^2}{R^2} \right) - \frac{\mu(\lambda^4 r^2 + R^2)}{3\lambda^2 r^2}, \quad t_{\vartheta z} = \mu \gamma \lambda r, \quad t_{\vartheta r} = 0 \quad (56)$$

$$t_{z\vartheta} = \mu \gamma \lambda r, \quad t_{zz} = \mu \left\{ \frac{2}{3} \lambda^2 - \frac{\gamma^2 r^2}{3} - \frac{1}{3} \left[\left(\frac{R}{\lambda r}\right)^2 + \left(\frac{r}{R}\right)^2 \right] \right\}, \quad t_{zr} = 0$$

Concrete relation between the blood vessel deformation (cross-section area A) and the boundary conditions, i.e. the transmural pressure $p_{in} - p_e$ and tension T_z we find applying the force balance on the external and internal vein surfaces in actual state. It can be formulated by Cauchy stress tensor only, i.e.,

$$\frac{\partial t^{ik}}{\partial x^k} = 0 \text{ for } x \in V \dots \text{ blood vessel, } i, k = r, \vartheta, z$$

$$p = p_{in} \text{ for } x \in \partial V_m \dots \text{ blood vessel internal wall} \quad (57)$$

$$p = p_e \text{ for } x \in \partial V_e \dots \text{ blood vessel external wall}$$

Providing that $t^{ik}(r)$ is the function of radial coordinate r only, the balance in the radial direction is

$$\frac{\partial t_{rr}}{\partial r} + \frac{t_{rr} - t_{\vartheta\vartheta}}{r} = 0 \quad (58)$$

the balance in the azimuthal direction

$$\frac{1}{r^2} \frac{\partial}{\partial r} (r^2 t_{r\vartheta}) = 0 \quad (59)$$

and the balance in the longitudinal direction

$$\frac{1}{r} \frac{\partial}{\partial r} (r t_{rz}) = 0 \quad (60)$$

From the relations (59) and (60) for the stress tensor elements it follows

$$t_{\vartheta r} = t_{r\vartheta} = \frac{d_\vartheta}{r^2}, \quad t_{zr} = t_{rz} = \frac{d_z}{r} \quad (61)$$

With respect to the definition of stress tensor (56) the constants are $d_\vartheta = d_z = 0$. The equation (58) is integrated through the thickness of the blood vessel wall

$$\int_{r_{in}}^{r_e} \frac{\partial t_{rr}}{\partial r} dr = t_{rr,e} - t_{rr,in} = \int_{r_{in}}^{r_e} \frac{t_{\vartheta\vartheta} - t_{rr}}{r} dr \quad (62)$$

We denote

$$t_{rr,e} = -p_e, \quad t_{rr,in} = -p \quad (63)$$

the external and internal pressure. With respect to the walls orientation in the external normal direction the pressure has effect in the opposite direction therefore the signs are minus.

The forces balance in the radial direction providing that there is not distortion, i.e. $\gamma = 0$, is

$$p - p_e = \int_{r_{in}}^{r_e} \frac{t_{\vartheta\vartheta} - t_{rr}}{r} dr = \mu \int_{r_{in}}^{r_e} \left[\frac{2r^2}{3R^2} - \frac{\lambda^4 r^2 + R^2}{3\lambda^2 r^2} - \frac{2}{3} \left(\frac{R}{\lambda r}\right)^2 + \frac{r^2 + \lambda^2 R^2}{3R^2} \right] \frac{dr}{r} \quad (64)$$

We introduce the substitution $\tilde{r} = \frac{r}{R}$ and by integration we get the final relation

$$p - p_e = \frac{\mu}{2} \left[\left(\frac{r_e}{R_e}\right)^2 - \left(\frac{r_{in}}{R_0}\right)^2 + \frac{1}{\lambda^2} \frac{R_e^2}{r_e^2} - \frac{1}{\lambda^2} \frac{R_0^2}{r_{in}^2} \right] \quad (65)$$

in which, we have to apply furthermore the mass conservation law which has for the cylindrical artery the form

$$R_e = R_0 + h_0, \quad r_e = r_{in} + h \text{ is valid } 2\pi R_0 h_0 = 2\pi r_{in} h \quad (66)$$

h_0 is the initial thickness of the wall. By the relations (66) we eliminate parameters R_e, r_e, h and neglecting the terms of the second order $\left(\frac{h_0}{R_0}\right)^2, \left(\frac{h_0}{r_{in}}\right)^2$ we derive

$$p - p_e = \frac{\mu h_0}{R_0} \left[1 + \left(\frac{R_0}{\lambda r_{in}}\right)^2 - \frac{r_{in}^2}{R_0^2} - \frac{R_0^4}{\lambda^2 r_{in}^4} \right] \quad (67)$$

The internal cross-section of the artery before deformation we denote A_0 and after deformation A , i.e.,

$$A_0 = \pi R_0^2, \quad A = \pi r_{in}^2 \quad (68)$$

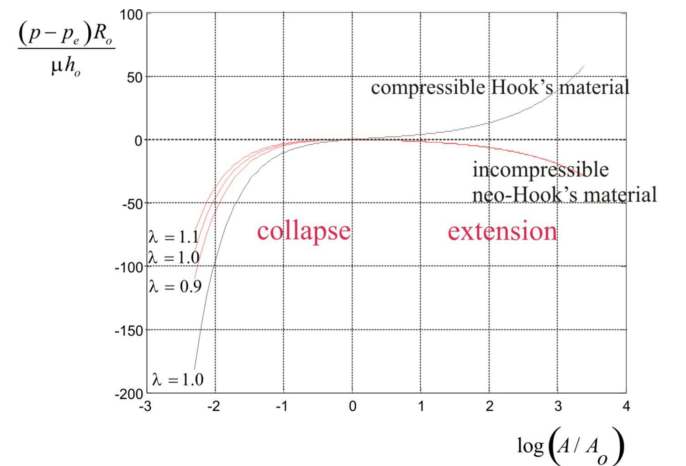


Figure 8 Dependence of the magnitude of the internal and external pressure difference $p - p_e$ within the blood vessel on the ratio of the arterial cross-sections A/A_0 for the compressible Hookean material (black line) and incompressible Neo-Hookean material (red line).

The final form of the balance of external forces on the internal and external arterial wall (64) including the elastic forces of the arterial wall is

$$p - p_e = \frac{\mu h_0}{R_0} \left[1 - \beta + \frac{1}{\beta \lambda^2} \left(1 - \frac{1}{\beta} \right) \right] = \Phi_{NH} \left(\frac{A}{A_0} \right) \quad (69)$$

$\beta = A/A_0$. The course of quantity $\frac{(p-p_e)R_0}{\mu h_0}$ characterizing the inflation or collapse is for the Neo-Hook material (56) obvious from the Figure 8. From here is evident that for this type of materials the artery (generally tube) can expand or collapse as well as at the internal pressure drop-off. This model is acceptable for the description of aneurysm, which can both increase and as well as decrease without occurring of the growth of internal pressure.

ANALYSIS OF THE COLLAPSE OF THE BRAIN BRIDGING VEINS

Provided that the elasticity of vein is given by the general formula

$$p - p_e = \Phi \left(\frac{A}{A_0} \right) \quad (70)$$

where A is the actual cross-section and A_0 is some referential resting cross-section when the blood does not flow. In the momentum equation (40) we replace the pressure gradient from the constitutive relation (70)

$$\frac{\partial p}{\partial x} = \frac{\partial \Phi}{\partial A} \frac{\partial A}{\partial x}, \text{ or } \frac{1}{\rho} \frac{\partial p}{\partial x} = c_0^2 \frac{\partial A}{A_0 \partial x}, \text{ for } c_0^2 = \frac{A}{\rho} \frac{\partial \Phi}{\partial A} \quad (71)$$

The equations (39) and (40) can be reformulate by relations (71) to the equations for $A(x,t)$, $v(x,t)$ only

$$\frac{\partial A}{\partial t} + v \frac{\partial A}{\partial x} + A \frac{\partial v}{\partial x} = 0 \quad (72)$$

$$\frac{\partial v}{\partial t} + v \frac{\partial v}{\partial x} + \frac{c_0^2}{A_0} \frac{\partial A}{\partial x} = -S \frac{\lambda_f}{8A_0} v |v| \quad (73)$$

The right side of the equation (73) represents the friction which can causes the flow damping only. The flow quality in the elastic tube is described by the left side of the equations (72), (73), i.e.,

$$\frac{\partial A}{\partial t} + v \frac{\partial A}{\partial x} + A \frac{\partial v}{\partial x} = 0 \quad (74)$$

$$\frac{\partial v}{\partial t} + v \frac{\partial v}{\partial x} + \frac{c_0^2}{A_0} \frac{\partial A}{\partial x} = 0$$

The system of these equations we will linearize, i.e., we assume that

$$\begin{aligned} v(x,t) &= v_0 + v'(x,t) \\ A(x,t) &= A_0 + A'(x,t) \end{aligned} \quad (75)$$

where v_0, A_0 are some constant values of the flow rate and the cross-section. The system of non-linear equations (74) transfer to the system of linear partial differential equations

$$\begin{aligned} \frac{\partial A'}{\partial t} + v_0 \frac{\partial A'}{\partial x} + A_0 \frac{\partial v'}{\partial x} &= 0 \\ \frac{\partial v'}{\partial t} + v_0 \frac{\partial v'}{\partial x} + \frac{c_0^2}{A_0} \frac{\partial A'}{\partial x} &= 0 \end{aligned} \quad (76)$$

The solution we will assume in the form of the sequential harmonic disturbances

$$\begin{pmatrix} A' \\ v' \end{pmatrix} = \begin{pmatrix} \bar{A} \\ \bar{v} \end{pmatrix} e^{i(\omega - kx)}, \quad \omega = \frac{2\pi}{T}, \quad k = \frac{2\pi}{\lambda} \quad (77)$$

with the amplitude \bar{A}, \bar{v} , with the time period T and the wave length λ . We are searching the condition at which the disturbances A', v' will be determined by the system of linear algebraic equations

$$\begin{aligned} (\omega - v_0 k) A' - A_0 k v' &= 0 \\ -\frac{c_0^2}{A_0} k A' + (\omega - v_0 k) v' &= 0 \end{aligned} \quad (78)$$

nonzero. The condition of existence of nonzero solution is

$$\det \begin{vmatrix} \omega - v_0 k & -k A_0 \\ -k \frac{c_0^2}{A_0} & \omega - v_0 k \end{vmatrix} = (\omega - v_0 k)^2 - k^2 c_0^2 = 0 \quad (79)$$

Therefore for the phase velocity of the disturbance is valid

$$\frac{\omega}{k} = v_0 \pm c_0 = \frac{\lambda}{T} \quad (80)$$

For collapsing tube is $T \rightarrow \infty$ and for the mean flow velocity we have the condition

$$v_0 = c_0 = \left(\frac{A_0}{\rho} \frac{\partial \Phi}{\partial A} \right)^{1/2} \quad (81)$$

For the Neo-Hook material (69) the speed of disturbance (pressure pulse) velocity is equal

$$\begin{aligned} c_{NH} &= \left(\frac{A_0}{\rho_0} \frac{\partial \Phi_{NH}}{\partial A} \right)^{1/2} = \left[\frac{h_0 \mu \left(\frac{1}{\lambda^2} - 1 \right)}{\rho R_0} \right]^{1/2} \\ &= \sqrt{\frac{1 \cdot 10^{-4} \cdot 4 \cdot 10^4}{10^3 \cdot 5 \cdot 10^{-3} (0.95^2 - 1)}} = 29 \text{ cm/s} \end{aligned} \quad (82)$$

The magnitude of this velocity corresponds to the conditions existing within the blood vessel. Therefore it is realistic that at some sudden movement of the head accompanied by slight shortening of the blood vessel, e.g. only about 5%, i.e. $\lambda = 0.95$.

Experimental set-up

The mock line in the Biomechanical Laboratory of the Czech Technical University in Prague is equipped with computer-controlled SuperPump pulsator, the software controls the pressure waveform and the frequency. Adjustable systemic resistor can be added to the circuit to adjust the smooth operation. The specimen is placed in the experimental chamber where the different external pressure and the axial pretension can be applied, see Figure 9. This set-up is used for detecting the pulse wave velocity in large arteries.

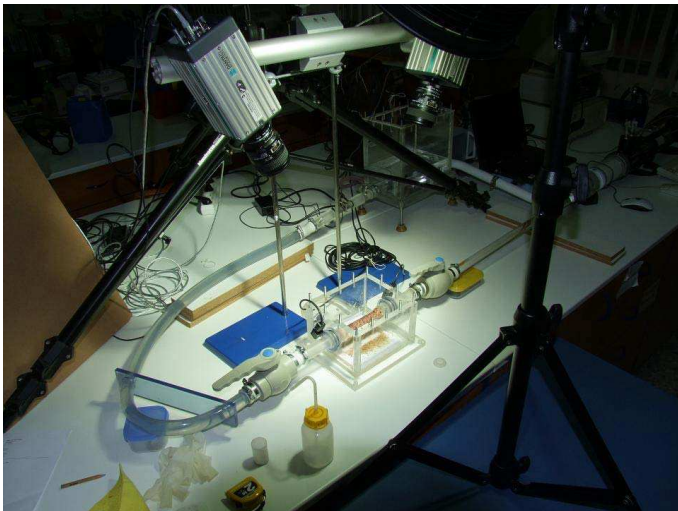


Figure 9. Two high-speed CCD cameras completed with 3D correlation system Q-450 can measure pulse wave velocity.

The fluid structure phenomenon is investigated both the continuous and pulsating flow is evaluated by non-invasive optical method and verified by the classical pressure measurement method. The radial displacements of the pulsating tube wall are evaluated optically. A crash test camera with high frame rate of 1000 Hz (fps) was used. The frame rate of 1000 Hz proved to be sufficient to register the high velocities of the pulse wave at short distances. Mentioned set-ups can also be used for static inflation-extension tests of elastic tubes with inner diameters in the range of 3 - 25 mm.

The investigation of the self-excited oscillations in elastic tubes is another purpose of the above equipments. It contains hydrodynamic pump that generates continual flow, stilling chambers for calming disturbances in the flow in front of and behind a specimen (portion of vein used in testing), see Figure 10.

8. COMPARISON WITH EXPERIMENTS

The experiments were done on a apparatus in Figure 10 with latex tubes with shear modulus $\mu = 0.5$ MPa of different thicknesses and diameters and with distilled water as the fluid. The pressure at the inflow p_1 and at the outflow p_2 of the flexible tube and the average fluid flow rate Q were measured. Stable self-excited low-frequency oscillations with the frequency f were observed, see Table 1.

In this table D_0 is the tube inner diameter, h is the tube thickness, L is the original tube length, L_{strained} is the corresponding prestrained length, p_e the outside pressure, the pressure drop on the flexible tube and f the frequency of the $\Delta p = p_2 - p_1$ observed self-excited oscillations. The obtained frequencies lie in the range of 0.2 - 5.6 Hz. However, not all observed oscillations were harmonic and regular, as reported in the table above, but some were irregular, without a main frequency. It is a quite delicate task to tune the experiment to the regime of regular self-excited oscillations. The frequency obtained by the numerical simulation for the shear modulus

$\mu = 10$ MPa was not regular, but it was close to the frequency 23 Hz. The discrepancy with the experiment is partially caused by the different shear modulus by anisotropy (19) and partially by the influence of the boundary conditions. The strong pressure pulsation affects partially the flow conditions in the whole experimental line. Nevertheless, taking into account the extreme sensitivity of this phenomenon, the agreement with above experiment is acceptable.

D_0 [mmHg]	h [mm]	L [mm]	L_{strained} [mm]	p_e [kPa]	$\Delta p = p_2 - p_1$ [kPa]	Q [L/s]	f [Hz]
10	0.85	95	-	2.4	0.5-0.7	0.060-0.062	2.5-3
10	0.85	95	-	3.3	0.4-1	0.065-0.067	2.9-4.3
10	0.85	95	-	5	0.6-1.2	0.056-0.058	4.3-5.6
14	1	145	181	0	1-3.5	0.092-0.25	1.9-5.4
14	1.2	140	175	0	1-5.1	0.143-0.383	1.9-5.6
20	0.85	172	-	1.9	0.2-1.5	0.095-0.98	0.2-0.6
20	0.85	172	-	5.8	0.4-4.8	0.093-0.095	0.2-0.6
20	0.85	172	-	9.8	1-5.4	0.092-0.093	0.2-0.6

Table 1. Experimental data with self-excited oscillations performed on the experimental set-up in the Figure 10.

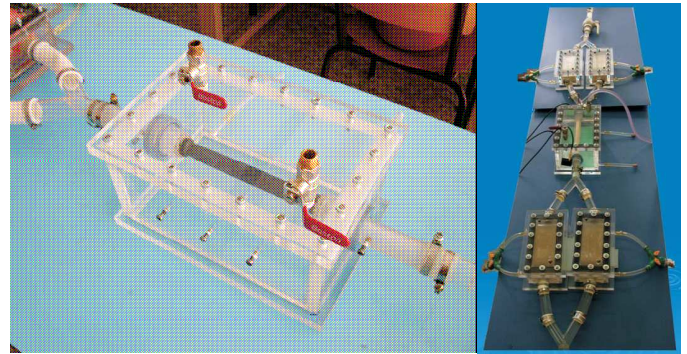


Figure 10. Left part-The flexible tube (vein) is placed in the pressurized chamber with the pressure p_e . Right part -Two stilling chambers satisfy nonreflecting conditions.

The clinical research of the bringing brain veins shows the existence of two type of venous brain systems; thin wall and thick wall veins. The elastic modulus of these veins is one order in magnitude difference. The high sensitivity of the thin wall veins on the blood flow rate and extension or contraction on their structural stability was observed. Moreover, the existence of continuing small wall vibration under physiological conditions was recognized too. The shear modulus μ provided experimentally in the scope of the small deformations was in the range $\mu = (2 \div 4) \cdot 10^4$ Pa and Young modulus $E = (0.6 \div 1.2) \cdot 10^5$ Pa. Due to the high hyperelasticity of the vein tissue, the ultimate stress reached the value $2 \cdot 10^7$ Pa and the specific elongation $\Delta l / l_0 = 0.25 \cdot 10^{-3}$ m. Prevailing inner diameters were in the range $(0.40 \div 5.85) \cdot 10^{-3}$ m and the

lengths $(4 \div 25) \cdot 10^{-3} \text{ m}$, the wall thickness of the bridging vein was $(0.1 \div 0.2) \cdot 10^{-3} \text{ m}$.

The total collapse of the thin bridging brain veins was observed under the flow conditions and can be with sufficient accuracy predicted by the formula (82). We can conclude that the simultaneous clinics observation (histological findings), in vitro experiments and numerical modeling gives sufficient data to predict biomechanical conditions of the angiosynizesis (the closing of the brain vein).

9. CONCLUSION

This paper open the way to the prediction of the biomechanical conditions (geometrical dimensions, viscoelastic properties of veins and blood fluid flow conditions) at which an unstable behavior or even the vein collapse can occur. It is shown the crucial role of the material and geometrical parameters of the vein walls with the respect of the fluid-structure phenomena, like pressure pulse propagation, self-induced oscillation, aneurysm growth etc. It was found, that the Neo-Hook's material model can be applied for the description of steady aneurysm form (volume). The question is now how described the tissue remodeling and corresponding changes of elastic parameters (e.g., shear modulus, vein radius and its wall thickness, etc.) As an example of this theory the conditions of the full collapse were formulated. It was shown, that the vein collapse can occurs, even under normal physiological condition in the case of the sudden stroke into the head.

The weak formulation is based on the principle of the extended virtual work and the further development of this approach to the implementation of the tissue remodeling on the base of biochemistry is open. The mixed formulation of the finite element method with the separately interpolated pressure is used for the structure. The above method allows to apply not only isotropic material but the anisotropy induced by the collagen structure can be taken into account.

The strong coupling between structure solver and fluid solvers allow to simulate large deflection oscillations of the structure. The detection of the onset of the stability is one of the most important features of this numerical code.

To compare the simulation with the adequate experiment is very difficult in general. The special experimental line was designed to fit and to check the accuracy of the simulation [7]. Latex tubes with variable inner diameter and wall thickness were used as specimens. Moreover, the pulse pressure test was performed with the human vein in vitro. The fluid structure phenomenon was investigated by the non-invasive optical method and verified by the invasive pressure method.

The special attention is devoted to the biomechanical properties of the bringing brain veins: the existence of two type of venous brain systems; thin wall and thick wall veins with the one order different elastic modulus magnitude the high sensitivity of the thin wall veins on the blood flow rate and extension or contraction on their structural stability the existence of continuing small wall vibration under physiological conditions. The simultaneous clinics observation (histological findings), in vitro experiments and numerical

modeling gives sufficient data to predict biomechanical conditions of the angiosynizesis.

ACKNOWLEDGEMENT

We gratefully acknowledge the support of the Czech Science Foundation No. 106/08/0557, and Ministry of Education, Youth and Sports of the Czech Republic, No. 1M06031.

REFERENCES

- [1] Shapiro A. H.: Steady flow in collapsible tubes, ASME J. of Biomechanical Eng. Vol. 99, (1977) 126-147.
- [2] Formaggia L., Quarteroni A., and Veneziani A.: Cardiovascular Mathematics, Modeling and simulation of the circulatory system, Volume 1, 2009, DOI: 10.1007/978-88-470-1152-6
- [3] Heil M.: An efficient solver for the fully coupled solution of large-displacement fluid-structure interaction problems, Computer Methods in Applied Mechanics and Engineering, 193, 2004, 1–23.
- [4] Hayashi S., Hayase T., Miura Y., Iimura I.: Dynamic Characteristics of Collapsible Tube Flow, JSME Inter.J., Vol. 42, No. 3, (1999) 689-696.
- [5] Maršík F., Převorovská S., Brož Z., Štembera V.: Numerical model of human cardiovascular system Korotkov sound simulation, Cardiovascular Engineering: An International Journal, Vol. 4, No. 2, (June 2004) 193-199.
- [6] Galdi G.P., Rannacher R.: Fundamental trends in Fluid-Structure interaction, Vol.1 World Scientific, 2010.
- [7] Chlup H., Macková H., Maršík F., Konvičková S.: Self-excited oscillations of an elastic tube, Proceedings of Human Biomechanics, Hrotovice: 2006. ISBN: 80-214-3232-2. 2006.
- [8] Štembera V.: Self-excited oscillations of elastic tubes induced by fluid-structure interaction, PhD Thesis, Faculty Math. and Physics Charles University in Prague, 2010